Figure S1: Absolute abundance distribution of *M. pneumoniae* proteins . Protein copy numbers span three orders of magnitude. Red bars indicate directly quantified proteins with labeled reference peptides.
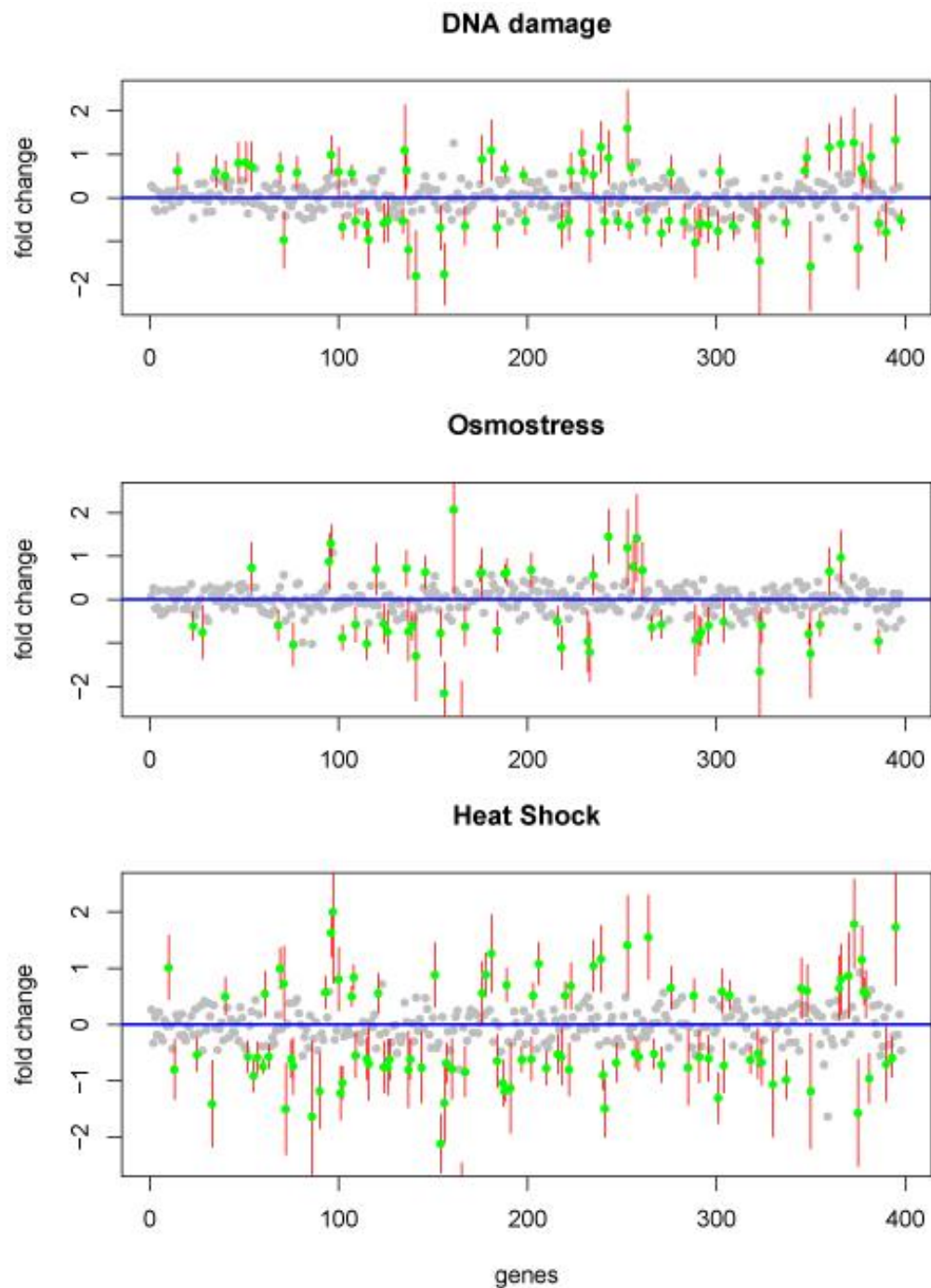
Figure S2: Proteome response profiles to cellular perturbations. Abundance changes of individual proteins in response to mitomycin C induced DNA damage, 0.5 M NaCl induced osmotic stress and to heat shock. Balls represent single proteins. Green balls indicate significant abundance changes in response to stress. Red vertical lines indicate the standard deviation of protein abundance under all conditions measured.
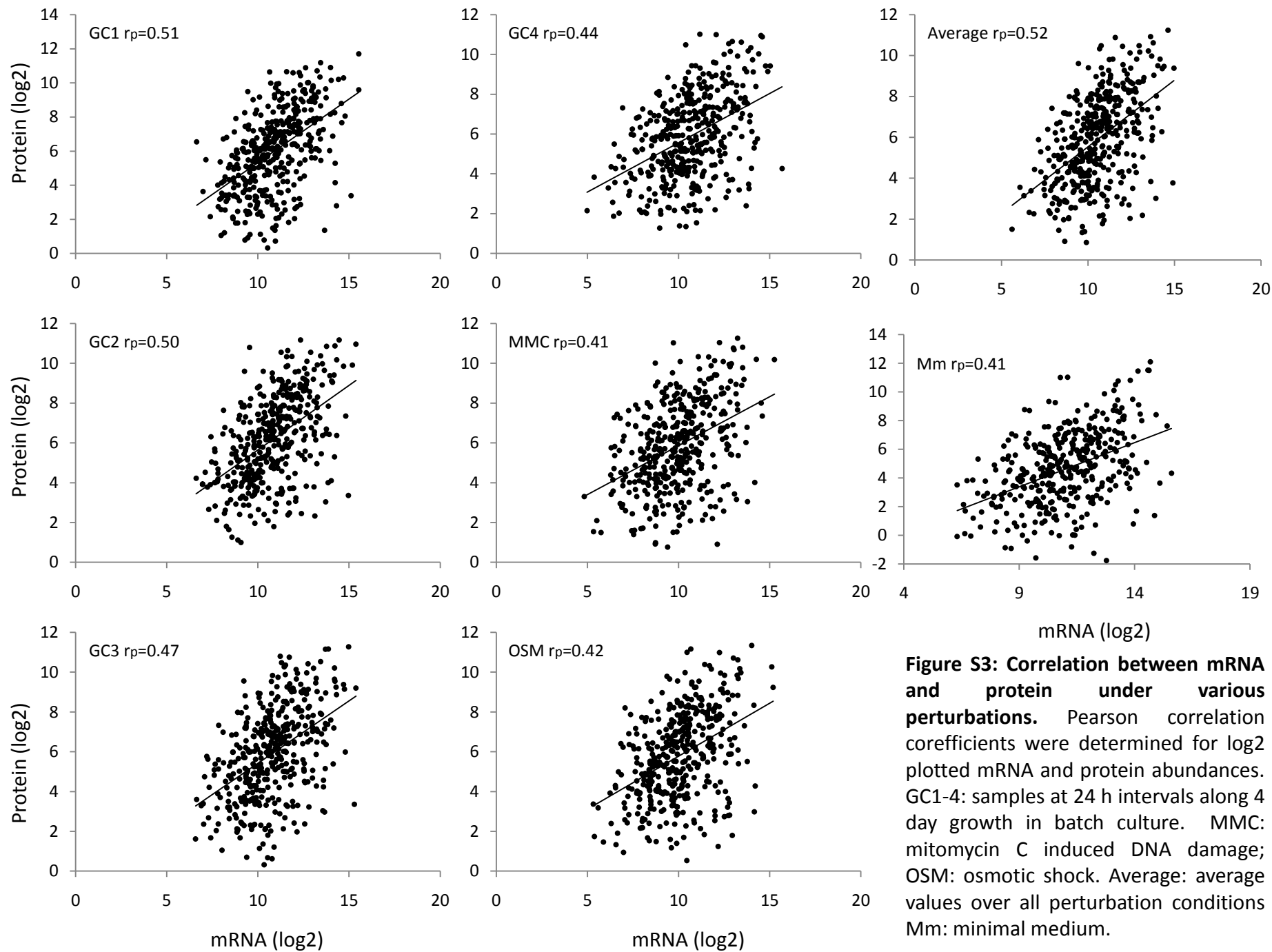
Figure S3: Correlation between mRNA and protein under various perturbations. Pearson correlation corefficients were determined for log2 plotted mRNA and protein abundances. GC1-4: samples at 24 h intervals along 4 day growth in batch culture. MMC: mitomycin C induced DNA damage; OSM: osmotic shock. Average: average values over all perturbation conditions Mm: minimal medium.
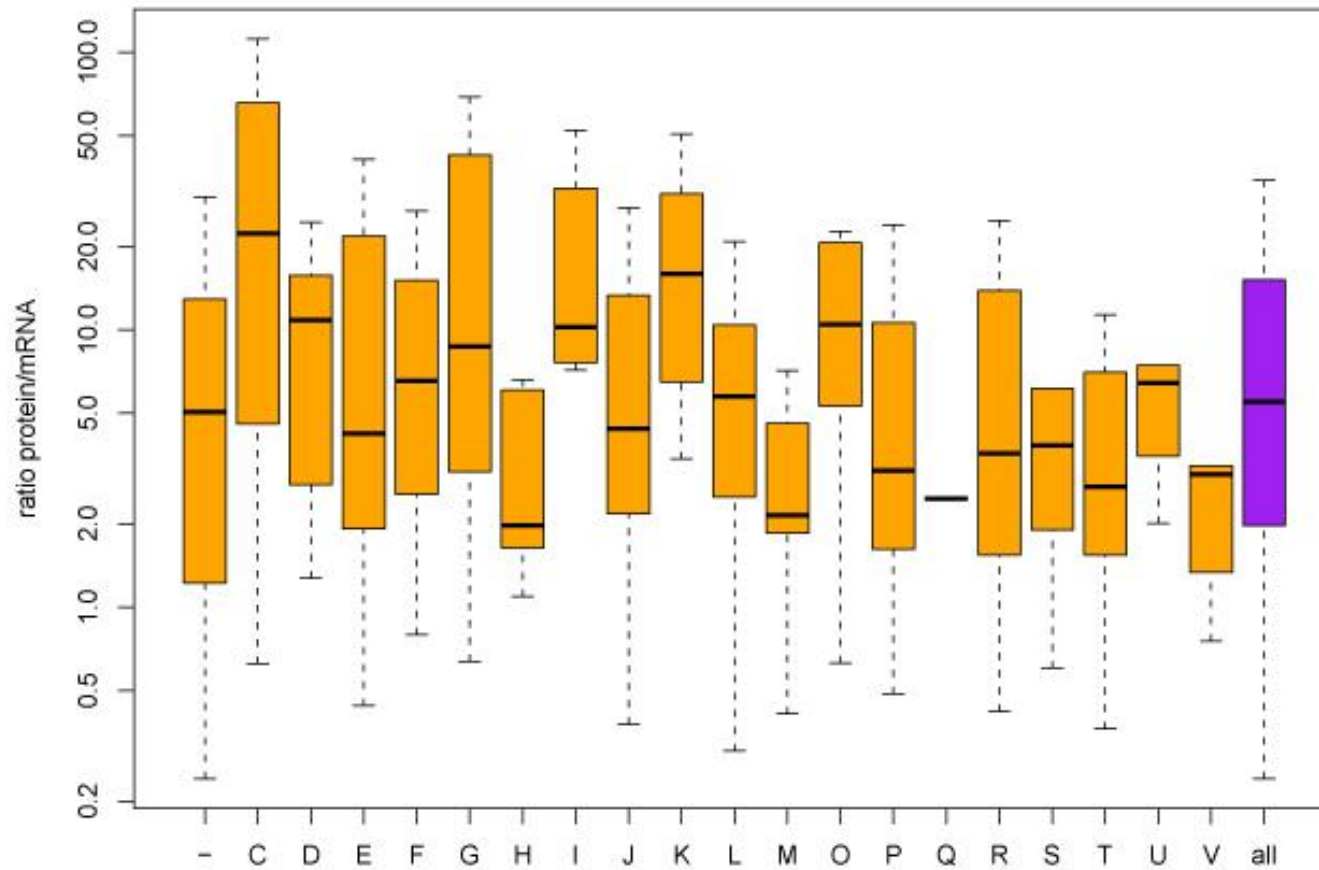
Figure S4: Boxplots for the ratio protein/mRNA copy number for the different genes in each of the general COG categories. Letters refer to COG classes. For certain classes (C, K) the protein/mRNA ratio appears increased. Others (V, M) appear to have lower protein/mRNA ratio than average. For protein number per class see table S2. For COG nomenclature see SI.
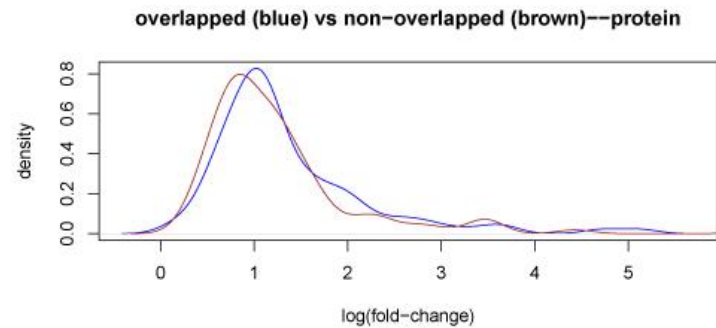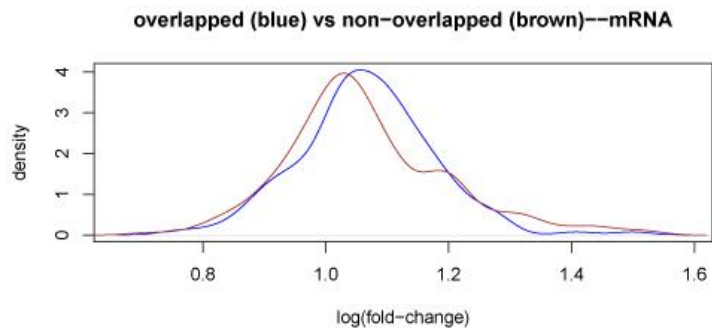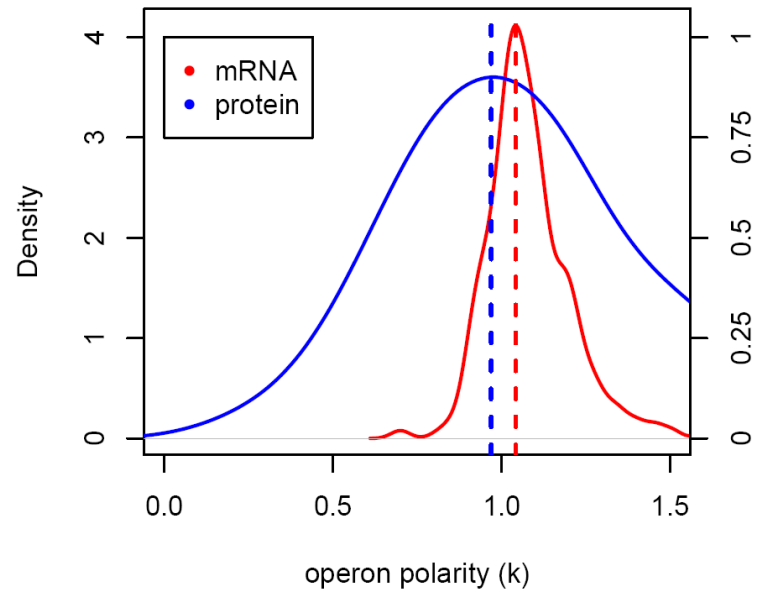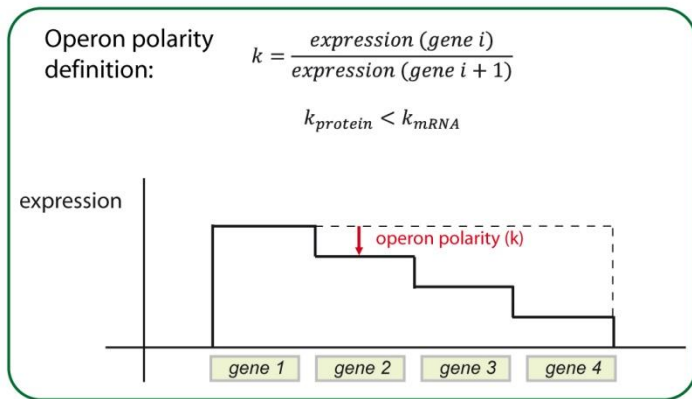
Figure S5: Operon polarity . Top left: Determination of operon polarity. Top right: Average operon polarity for proteins is below 1, indicating compensation for the observed staircase behavior on the transcript level. Bottom panels: operon polarity is measured for genes within polycistronic operons separately for overlapped and non-overlapped genes. No significant difference has been observed between the two operon classes.
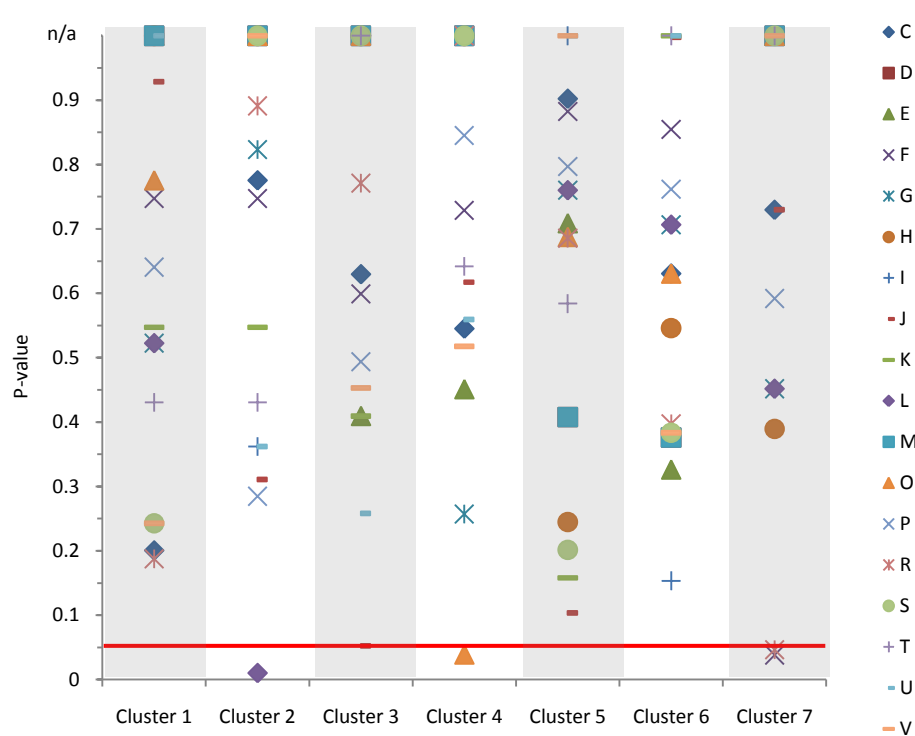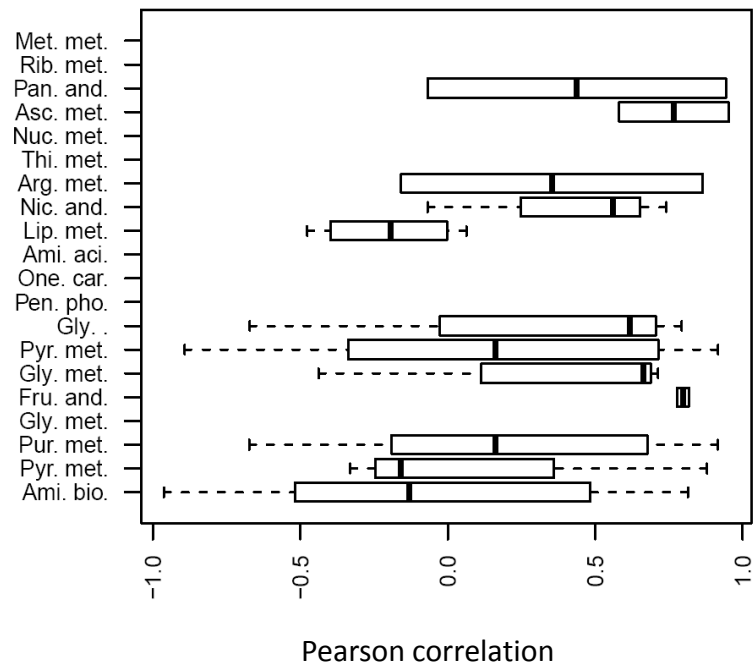
Figure S6. Functional analysis of mRNA-protein correlation along the growth curve. A: Fischer tests of functional classes within mRNA-protein correlation clusters. Significant enrichment in cluster 2: COG class L (5); in cluster 3: COG class J (8); in cluster 4: COG class O (5); in cluster 7: COG classes F (5), R (5). The meaning of COG class letters is detailed in the SI. **B:** Test for functional enrichment of mRNA-protein correlations along the growth curve. Met mat: Methionine metabolism; Rib met: Riboflavin metabolism; Pan and: Pantothenate and CoA biosynthesis; Asc met: Ascorbate metabolism; Nuc met. Nucleotide metabolism; Thi met: Thiamine metabolism; Arg met: Arginine metabolism; Nic met: Nicotinate and nicotinamide metabolism; Lip met: Lipid metabolism; Ami aci: Amino acid metabolism; One car: One carbon pool by folate; Pen pho: Pentose phosphate pathway; Gly: Glycolysis; Pyr met: Pyruvate metabolism; Gly met: Glycerophospholipid metabolism; Fru and: Fructose and mannose metabolism; Gly met: Glycolipid metabolism; Pur met: Purine metabolism; Pyr Met Pyrimidine metabolism; Ami bio: Aminoacyl–tRNA biosynthesis. Bars are missing for metabolic pathways where data was not sufficient.
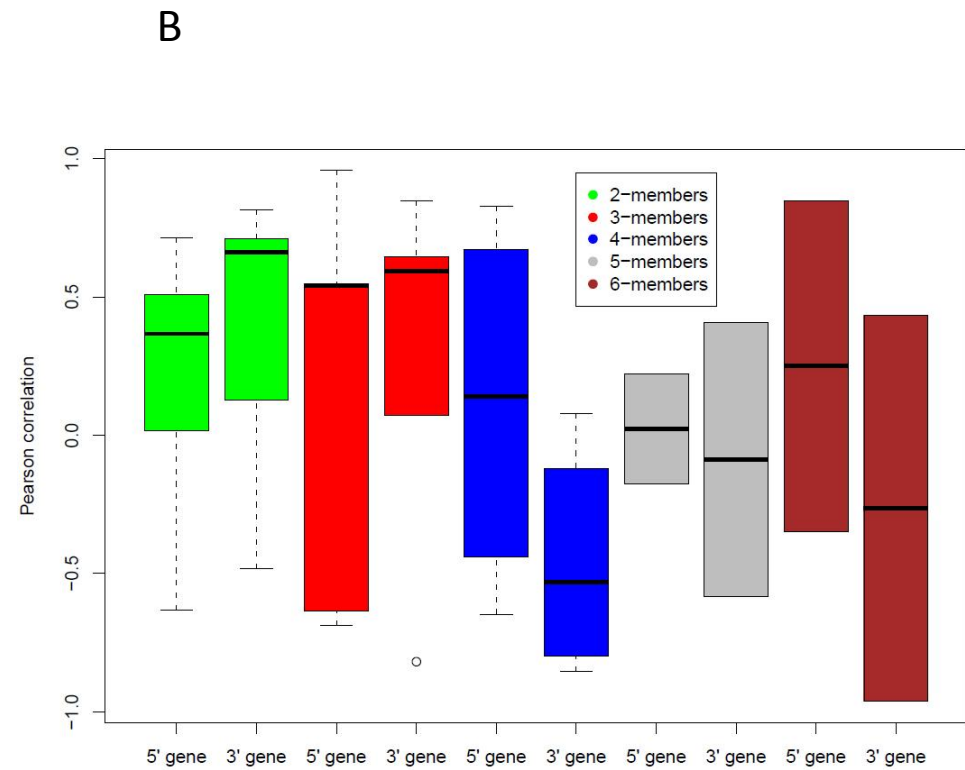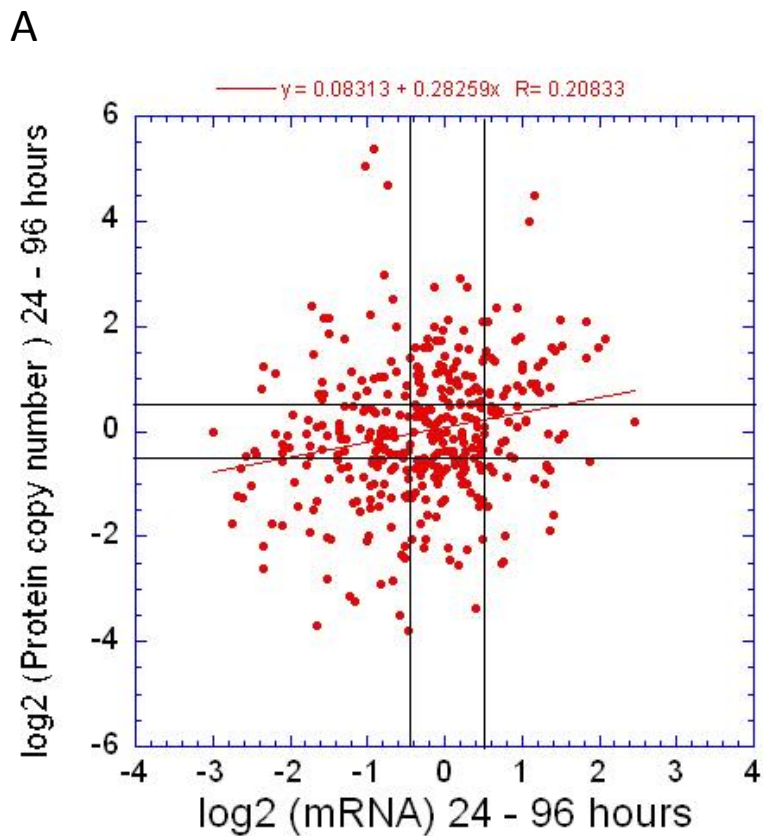
Figure S7: Analysis of mRNA-protein correlation during four day growth. A: mRNA-protein correlation for 24 h and 96 h timepoints. Top right and bottom left quadrant: concerted mRNA protein changes. **B:** mRNA-protein correlation coefficients along four day growth are related to gene topology. Subtle positional (5' or 3') and operon length related effects are observable.
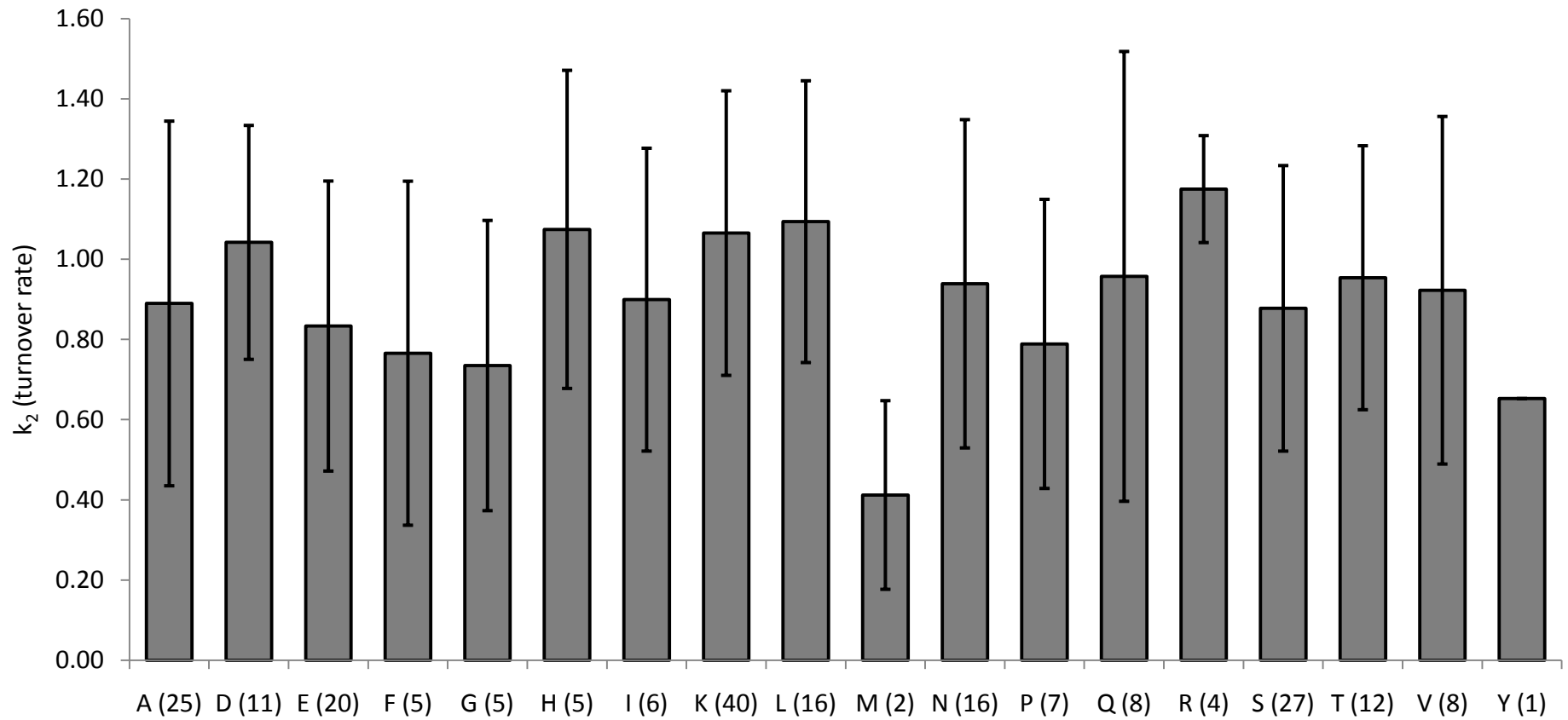
Figure S8: The N-end rule does not predict turnover rates for M. pneumoniae proteins. Proteins were binned according to the amino acid following the initial methionine. Numbers in brackets indicate bin sizes. Error bars refer to turnover rate standard deviation within the respective bin. Proteins with Cystein (C) or Tryptophane (W) after the initial methionine were not among the set of proteins with determined turnover rates.
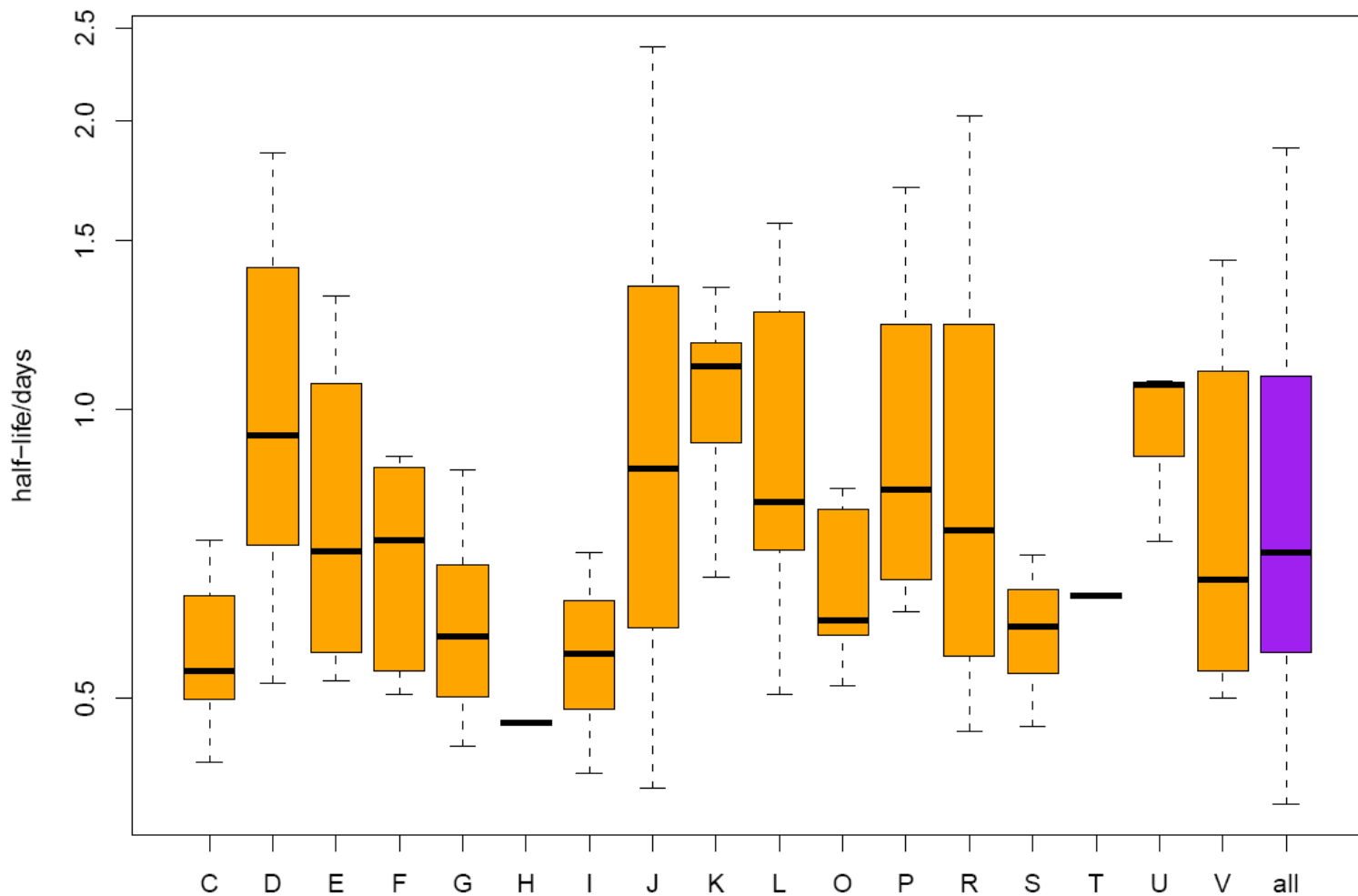
Figure S9: COG classification of proteins with determined half lives. Proteins with determined half-life were binned according to their COG functional class (table S4). COG class U (8 members) and K (12) have on average longer half lives than classes C (19), I (7) and S(14). Some outliers cannot be interpreted appropriately because of small bin size. For COG nomenclature (letters on X-axis) see SI.
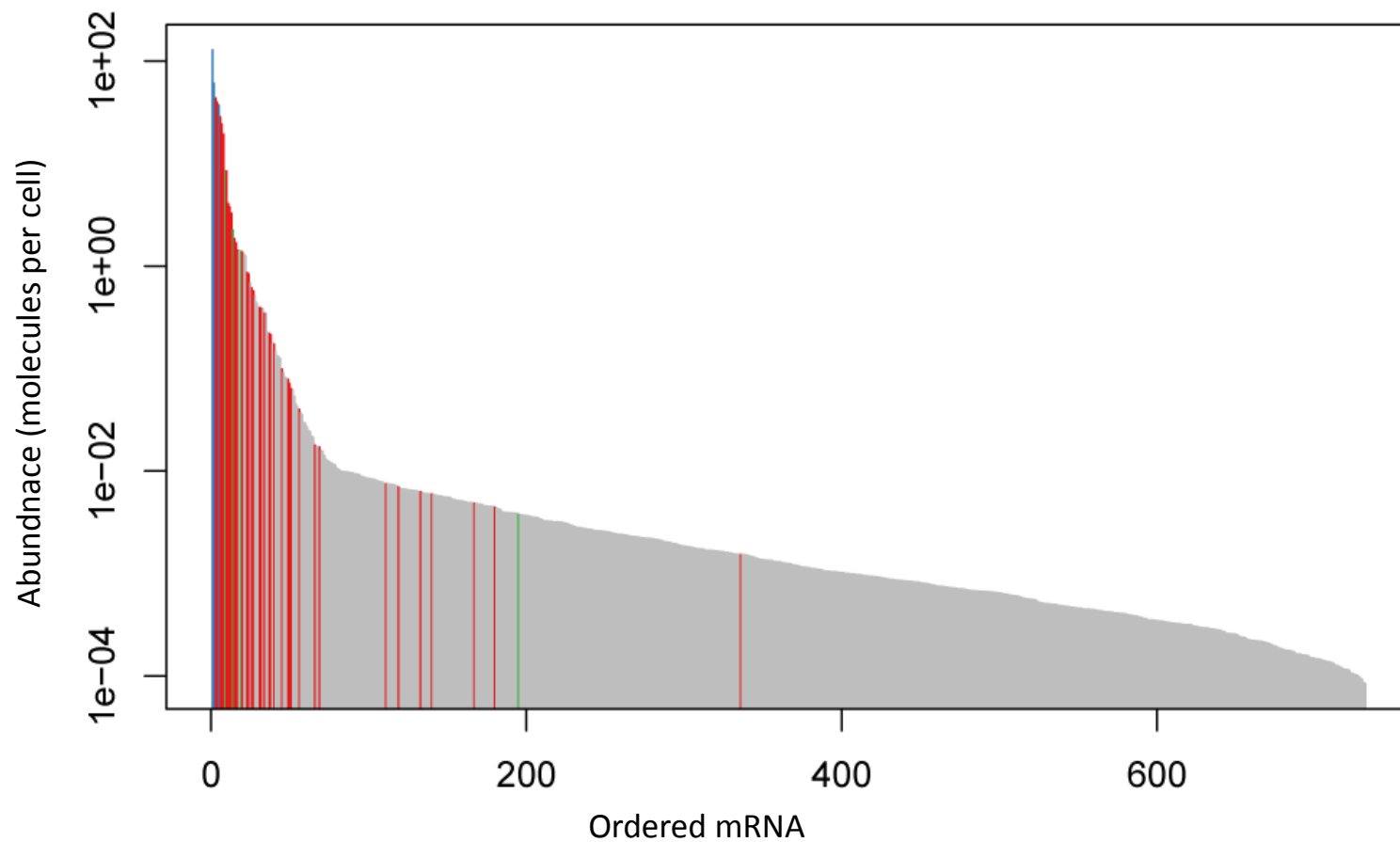
Figure S10: Absolute abundance distribution of cellular RNA. Blue: ribosomal RNA ; red: tRNA; green: other structural RNA, grey: mRNA. Celluar absolute abundance of mRNA is below one copy per cell for almost all mRNAs.
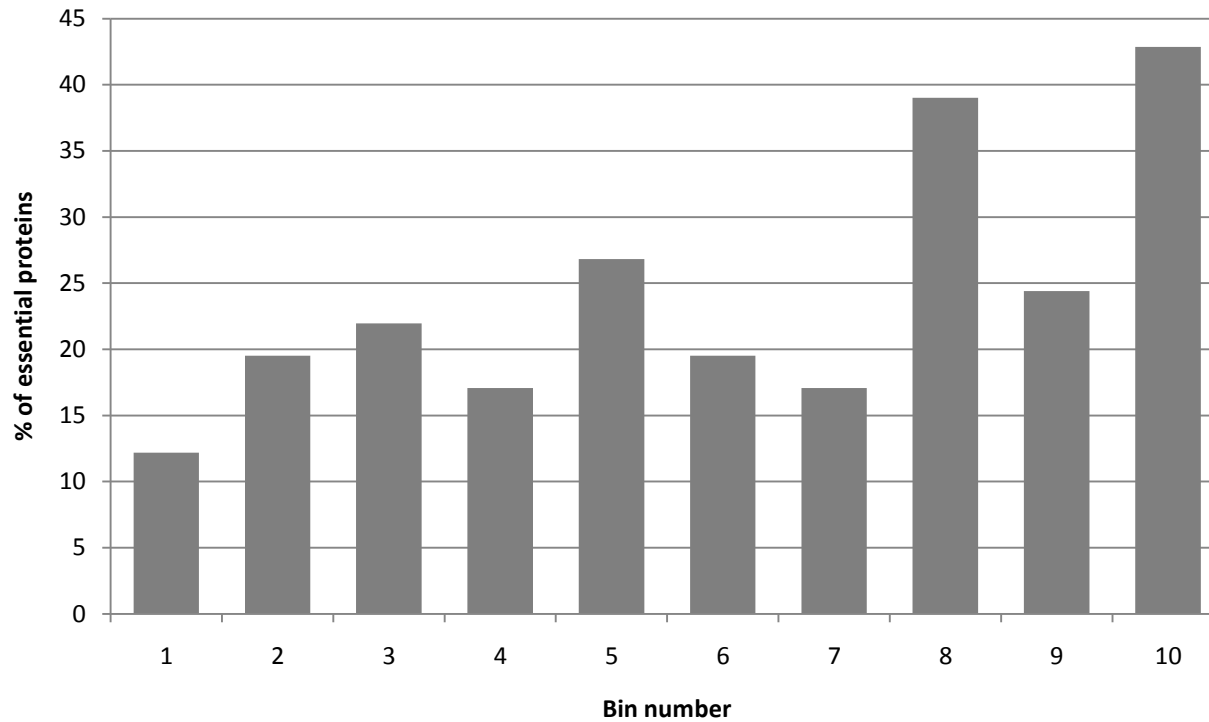
Figure S11: Low abundant proteins are less likely to be essential. Orthologs to proteins predicted as essential in the related bacterium Myocplasma genitalium were binned ($N_{bin}=41$) according to their abundance. % of essential proteins per bin indicates that high abundant proteins are enriched in essential proteins.
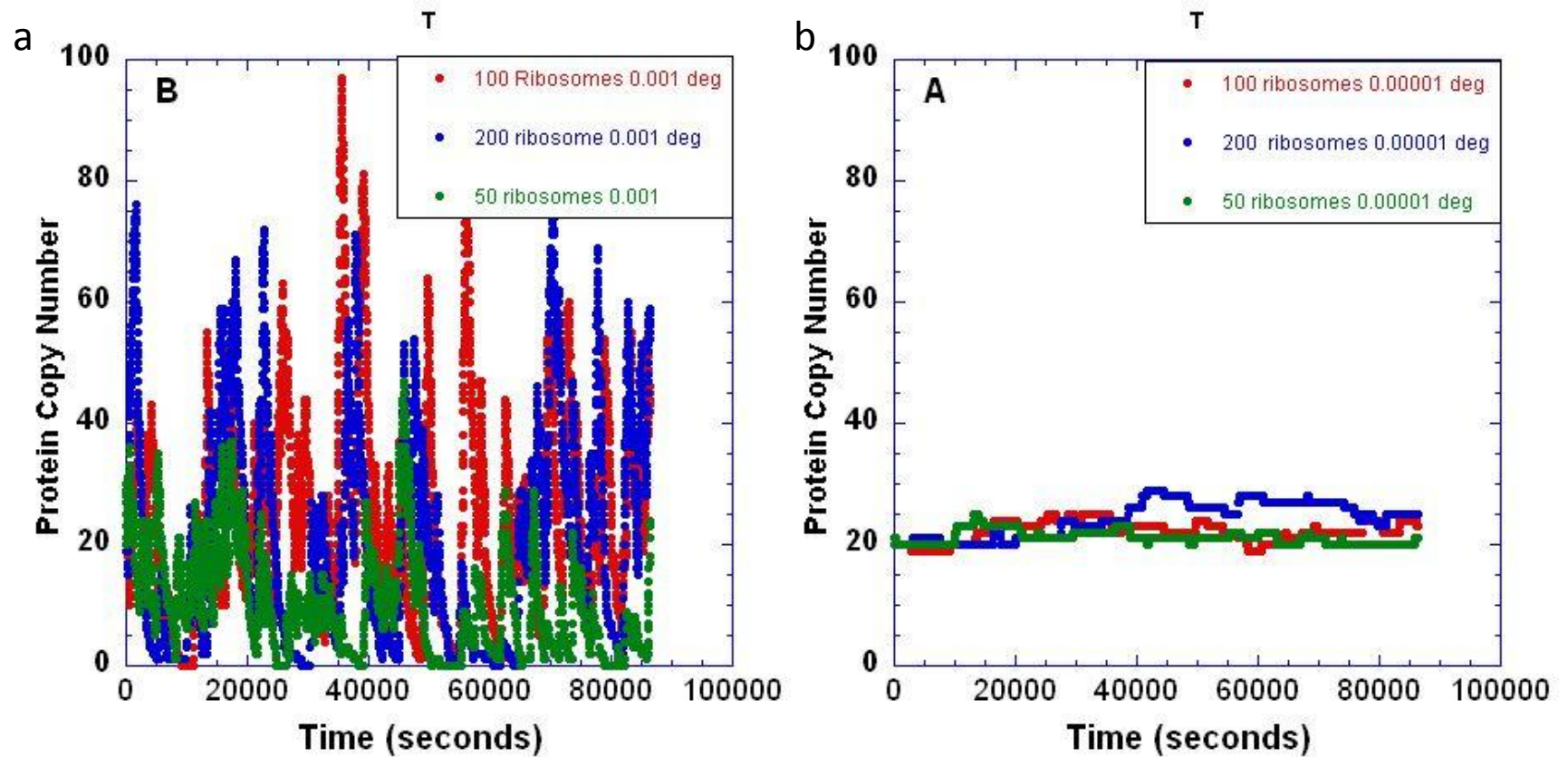
Figure S12: Stochastic simulations of protein abundance with different ribosome concentrations. Reducing ribosome number to 50 copies per cell as measured for cells grown in minimal medium conditions slightly reduces the abundance for proteins with fast turnover rates (a) but has only marginal effects on stable proteins (b).
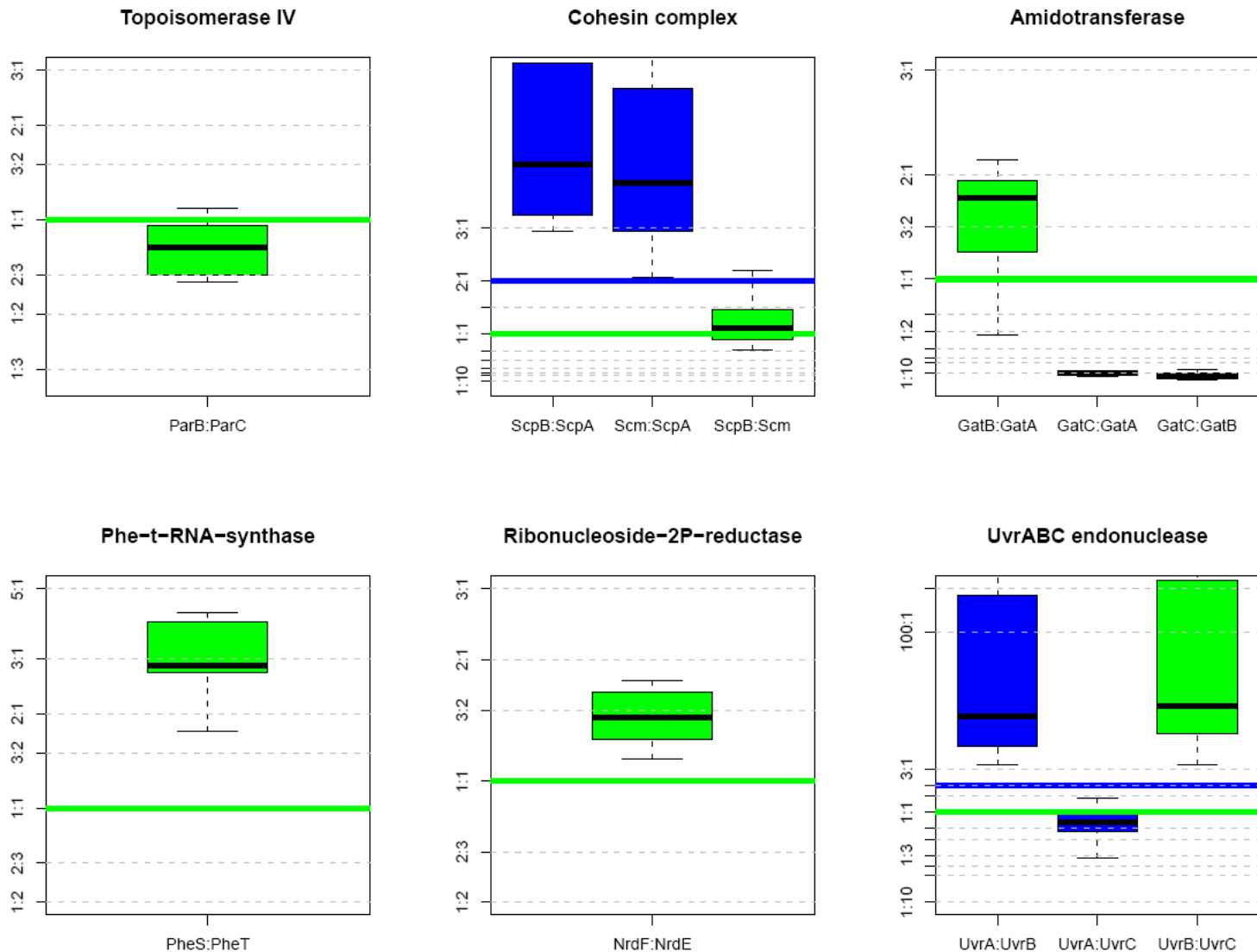
Figure S13: Further examples for protein complexes and the stoichometric abundance of the subunits in the proteome. Boxplots represent measured pairwise protein copy number ratios distributions within protein complexes. All different experimental conditions were used to estimate the distributions. Horizontal continuous lines represent expected stoichiometries. Identical colors associate the measured ratios (boxplots) with expected ratios from literature (horizontal lines).
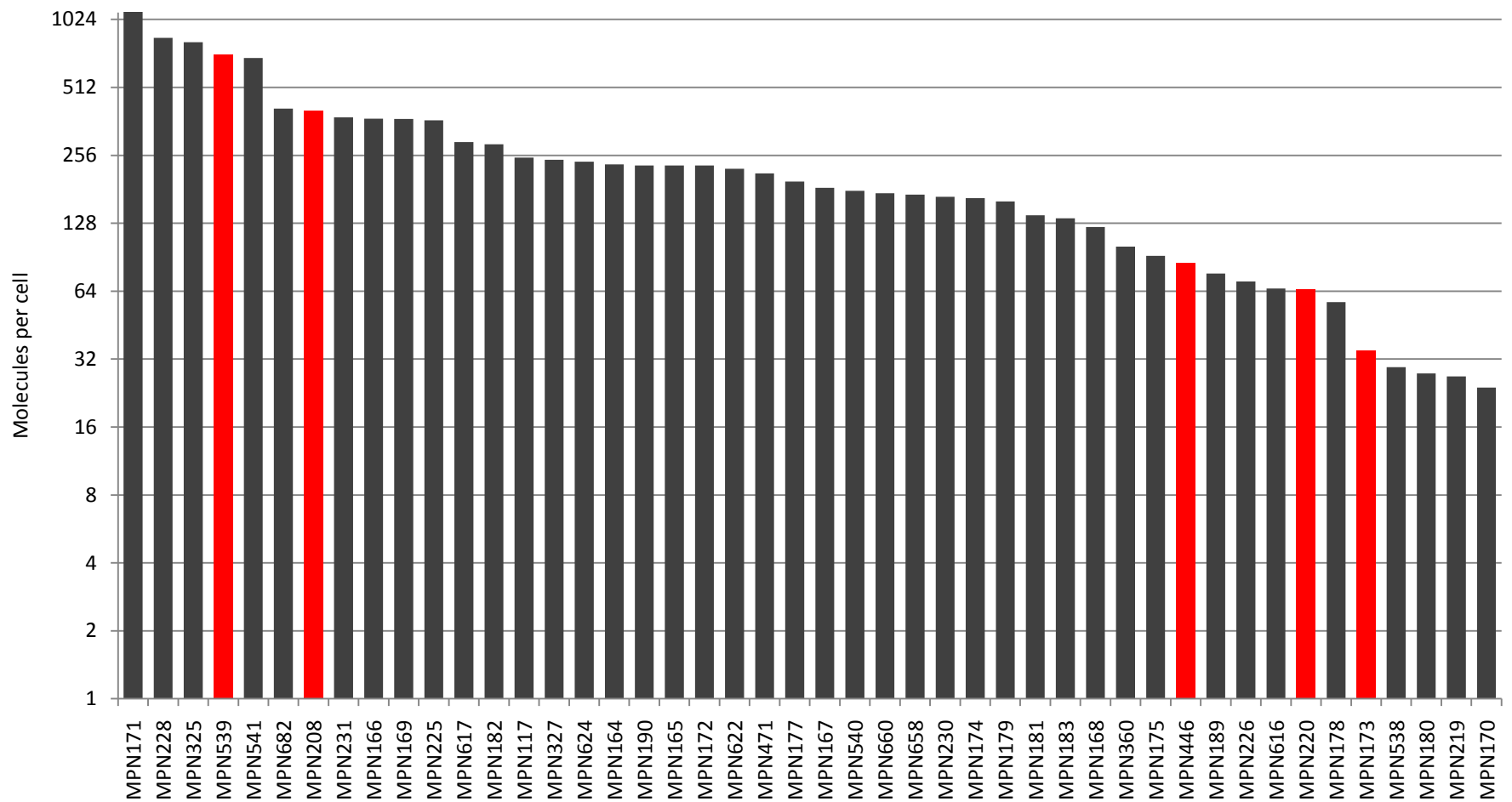
Figure S14: Abundance distribution of ribosomal proteins. Bars indicate the abundance of 46 quantified ribosomal proteins in molecules per cell. Red bars indicate proteins with confirmed abundance by quantitative Western blotting.
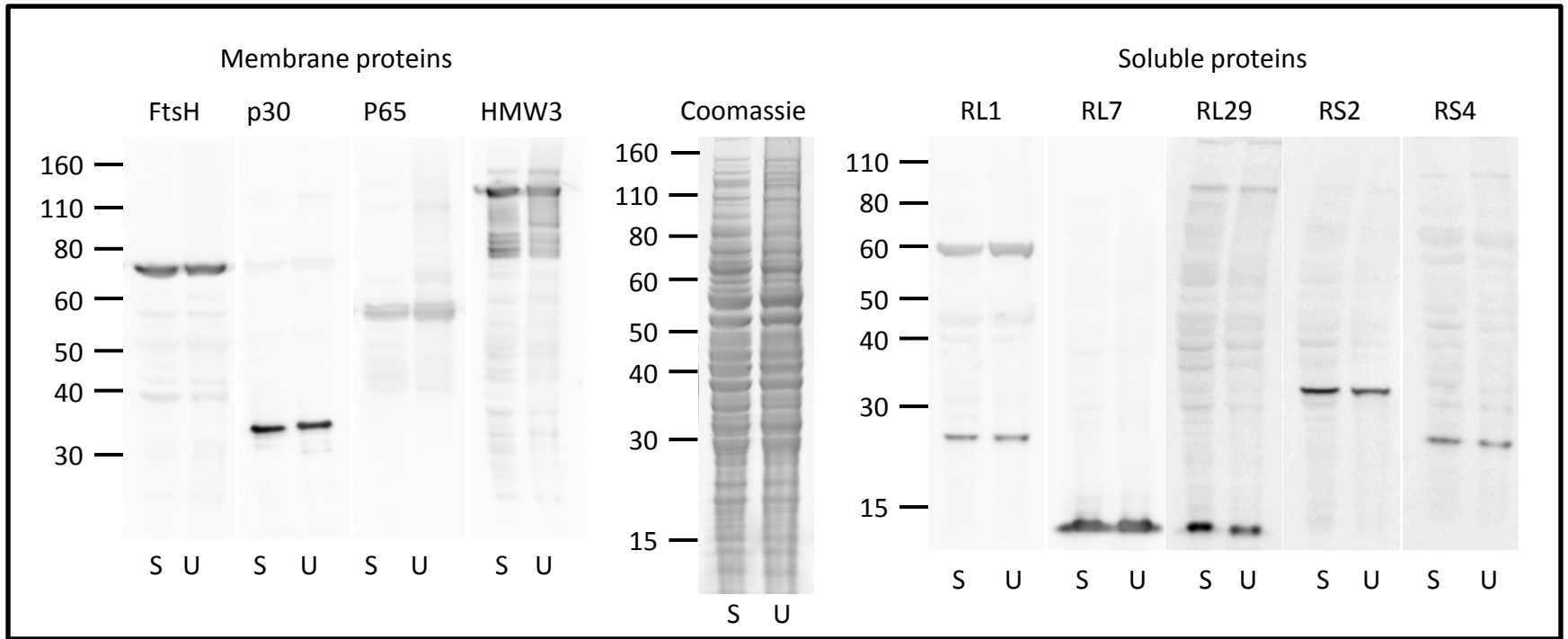
Figure S15: Comparison of cell lysis and protein resolubilization efficiencies of SDS (S) and urea (U) containing buffer. Left pannels: Western blots against proteins with several transmembrane helices (FtsH, p30, P65) or exclusive membrane localization (HMW3). Middel pannel: SDS-PAGE analysis of cell lysates containing either 4% SDS (S) or 8 M urea (U). Right pannels: Western blots against ribosomal proteins with cytosolic location.
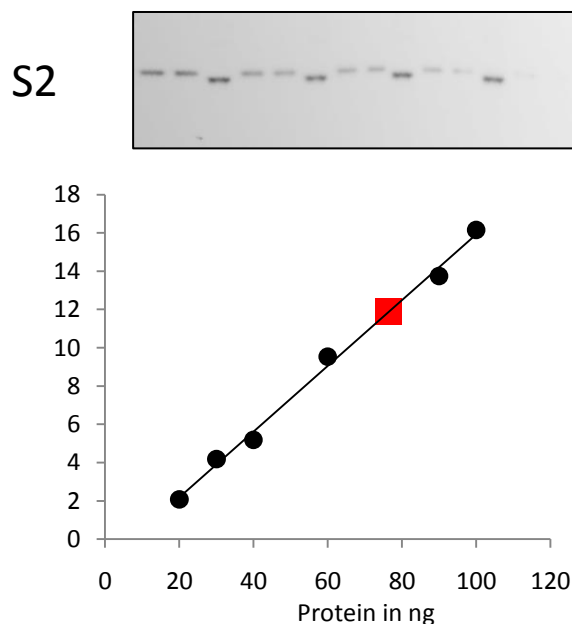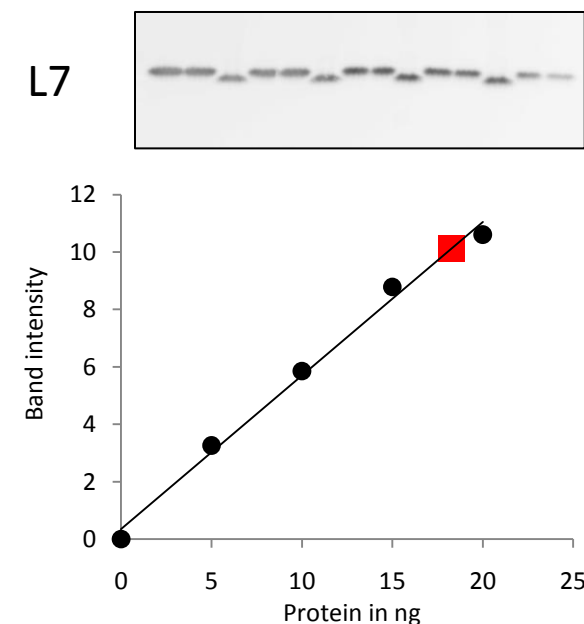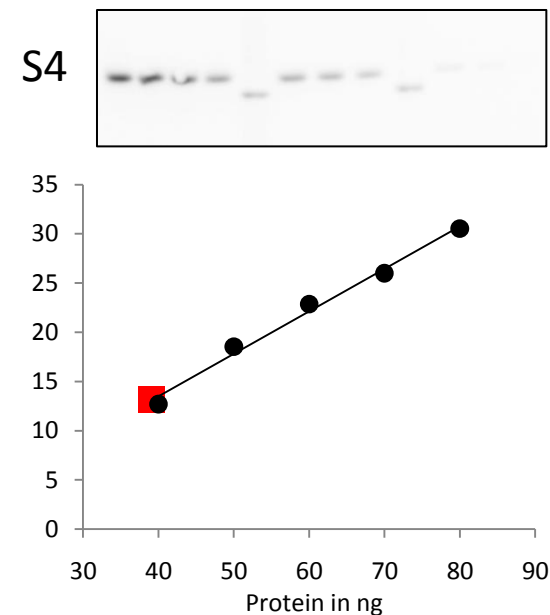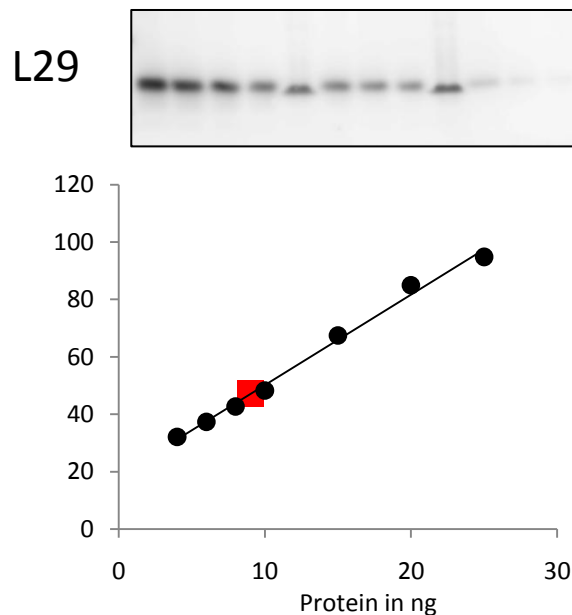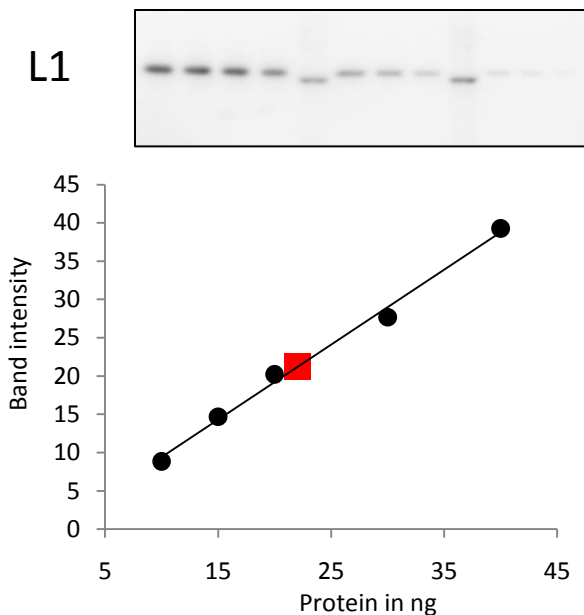
Figure S16: Quantitative Western Blots. 5 ribosomal proteins were quantified by quantitative Western blotting. X-axis: ng protein; Y-axis: intensity. Black circles are selected data points from directly representing Western blot intensities of the panels above. Red squares indicate intensities and abundances of the respective protein in a M. pneumoniae cell lysate. Calculations are described in the SI. Ribosomal proteins were purified with an affinity tag and therefore run at higher molecular weigths in SDS-PAGE.
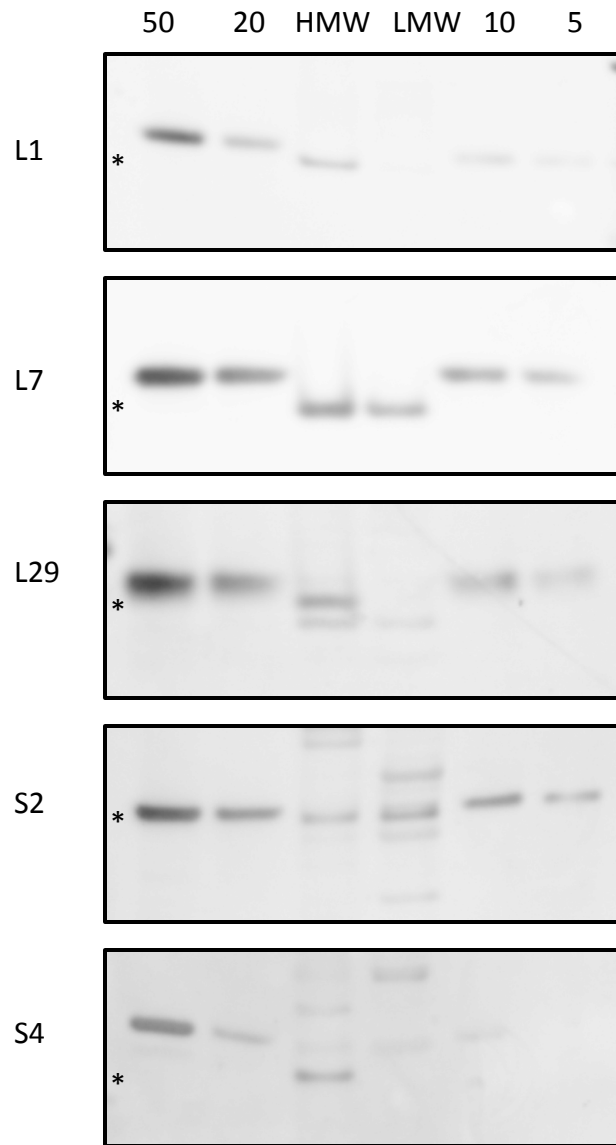
Figure S17: Western blots of size exclusion chromatrography fractions. Pooled high molecular weight fractions (HMW) corresponding to the size of ribosome particles and low molecular weight fractions (LMW) corresponding to the size of monomeric ribosomal proteins where analysed by Western blotting. For abundant ribosomal proteins L7 and S2, partitioning into HMW and LMW fractions is detectable. Comparing band intensities with purified ribosomal protein (50, 20, 10, 5 ng) shows that ribosomal proteins in HMW fractions present in approximately equal amounts. Ribosomal proteins were purified with an affinity tag and therefore run at higher molecular weigthts in SDS-PAGE. Corresponding bands in the size exclusion fractions are indicated with a star.
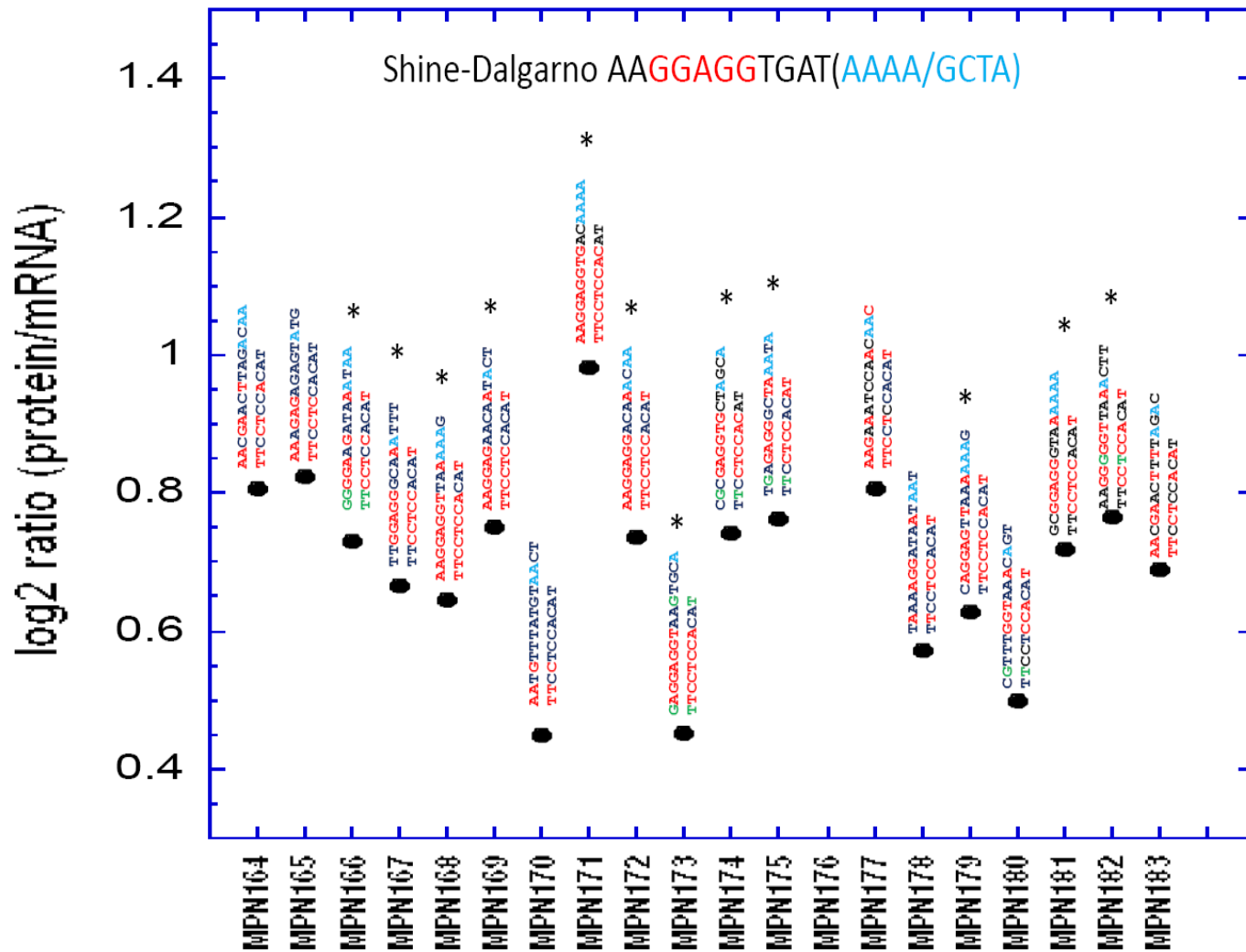
Figure S18: Post-transcripional control for ribosomal protein abundance. Plot displaying the ratio of the log2 values for Protein and mRNA copy numbers per cell for the main ribosome operon and its Shine-Delgarno sequences. The Shine-Delgarno sequence is shown for every gene above each ratio. Red colours correspond to base pairing. Green colour to GT base pairs allowed in RNA duplex and blue colour to the AAAA stretch frequently observed in *E. coli* at position +4 of the Shine-Delgarno sequence. The asterisk points out those sequences with at least 4 out of the 5 key GGAGG Shine-Delgarno sequence bases. Those not having an asterisk could have poor sequences, or use alternative non-canonical ribosome binding sequences. It should be noted that MPN171 with >1000 copies per cell (five times more than the median for ribosome proteins) has an optimal Shine-Delgarno sequence.
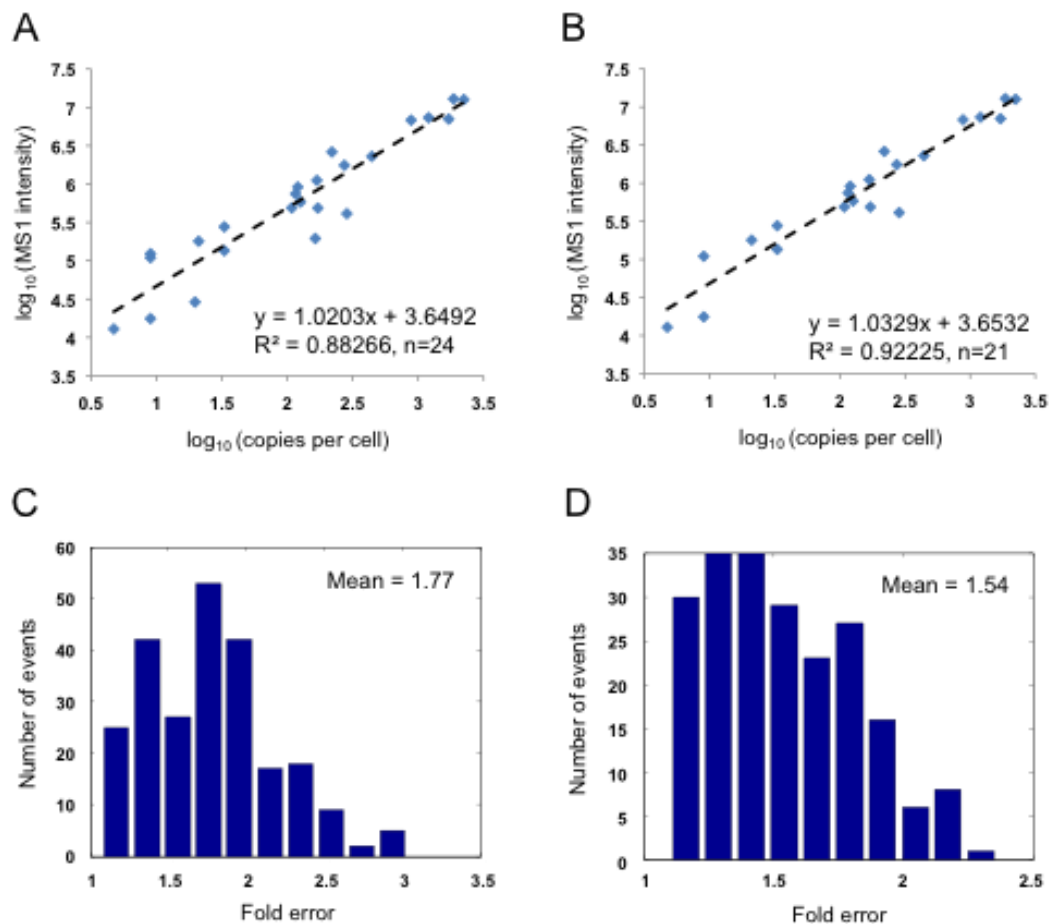
Figure S19: Correlation between protein MS1 intensities and their absolute abundances. (A) Logarithm of the averaged intensities of the up to three most intense peptide ions for 24 reference proteins plotted against the logarithm of copies/cell as measured by isotope dilution. (B) Like A, but restricted to 21 of these proteins, for which three unique peptide sequences could be identified (n=21). (C) Fold error distribution estimated by bootstrap analysis for all 24 proteins. (D) Like C for the 21 proteins being identified with at least 3 unique peptides.